

Invariant percolation properties in random isotropic systems of conductive discorectangles on a plane: From disks to sticks

Yuri Yu. Tarasevich* and Andrei V. Eserkepov†

Laboratory of Mathematical Modeling, Astrakhan State University, Astrakhan 414056, Russia

(Dated: June 20, 2022)

Recently, some eccentricity-invariant properties of random, isotropic, two-dimensional (2D) systems of conductive ellipses have been reported [Phys. Rev. B **104**, 184205 (2021)]. Moreover, the authors suggested that this invariance might also be observed in systems with other particle geometries having zero-width sticks as the limiting case. To check this suggestion, we studied 2D random systems of isotropically-placed, overlapping, identical discorectangles (stadia) with aspect ratios ranging from 1 (disks) to ∞ (zero-width sticks). We analyzed the effect of the aspect ratio and the number density of conductive discorectangles on the behavior of the electrical conductivity, the local conductivity exponent, and the current-carrying backbone. Our own computer simulations demonstrate that some of the properties of random, isotropic 2D systems of conductive discorectangles are insensitive to the aspect ratios of the particles.

I. INTRODUCTION

The 2D systems of randomly-placed, metallic nanowires and nanorods are being extensively studied. The interest in these systems is inspired by their combination of high electrical conductivity with excellent optical transparency that is in demand in numerous technological applications [1, 2] such as touch screens [3], transparent heaters [4], solar cells [5], and flexible electronics [6].

To mimic the shape of elongated particles and, at the same time, simplify the simulations, different simple geometrical figures are used, e.g., zero-width sticks (rods) [7–9], rectangles [10], ellipses [11, 12], superellipses [13], and discorectangles (stadia) [14]. Comparisons of some of the properties of random 2D systems of the above particles have been collected in Ref. [15]. The electrical properties of the 2D systems of randomly-placed conductive particles of the above shapes have also been studied [12, 16–18], with the greatest attention being paid to the simplest shape, i.e., to zero-width sticks [19–21], and the particular case when only the junction resistance is taken into account [22].

Some eccentricity-invariant properties of random isotropic, two-dimensional (2D) systems of conductive ellipses have recently been reported [12]. The authors have suggested that this invariance might also be observed in systems with other particle geometries having the zero-width sticks as the limiting case. To check this conjecture, we studied 2D random isotropic systems of conductive overlapping discorectangles. Their aspect ratios ranged from 1 (disks) to ∞ (zero-width sticks). We analyzed the behavior of the electrical conductivity, the local conductivity exponent, and the backbone in respect of the aspect ratio and the number density of these conductive discorectangles. We have compared our results

with the published results for ellipses [12] and sticks [16].

The rest of the paper is constructed as follows. Section II describes some technical details of our simulation. In Section III, we present our main results and discuss some open questions. Section IV summarizes the main results and suggests possible directions for further study.

II. METHODS

A. Sampling

A discorectangle (a stadium) is a rectangle with semi-circles at a pair of opposite sides (Fig. 1). Its aspect ratio is

$$\varepsilon = \frac{l}{d}. \quad (1)$$

When $\varepsilon = 1$, a discorectangle reduces in a disk. The limiting case $\varepsilon = \infty$ corresponds to a zero-width (widthless) stick.

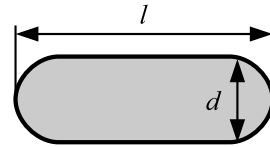


FIG. 1. Discorectangle (stadium).

Basically, in our study we used discorectangles with four alternative values of the aspect ratio, viz., $\varepsilon = 1, 7, 20, \infty$, while the discorectangle's length was fixed, $l = 1$. Some additional investigations have been performed for intermediate values of ε . Identical, permeable discorectangles with the chosen value of aspect ratio were randomly placed on a substrate. Their centers were independent and identically distributed within a square domain of size $L \times L$, while their orientations were equiprobable. To reduce the finite-size effect, periodic boundary

* Corresponding author: tarasevich@asu.edu.ru

† dantealigjery49@gmail.com

conditions (PBCs) were applied along both mutually perpendicular directions (Fig. 2).

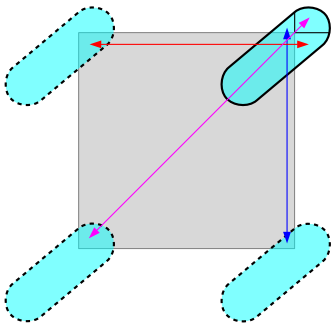


FIG. 2. Example of the effect of PBCs for the most complicated case. The discorrectangle in the top right corner extends beyond the square domain $L \times L$. Due to the PBCs, the parts of the particle that are outside the domain are duplicated in the remaining corners of the domain (these “ghost” particles are indicated using dashed lines).

The number density of the deposited particles is the number of particles N per unit area, i.e.,

$$n = \frac{N}{L^2}. \quad (2)$$

Another widely used quantity to characterize a deposit is the total area fraction of the deposited particles,

$$\eta = An, \quad (3)$$

where A is the area of each particle. In contrast to open boundary conditions, PBCs ensure that the relation (3) is exact. In the case of elongated particles, PBCs ensure the isotropic deposition of such particles, while the closed boundary conditions force the particles to align along the boundaries, which leads to locally anisotropic systems.

B. Overlapping of the deposited particles

Two discorrectangles are considered as connected if they overlap. The overlapping occurs when the center of the second discorrectangle is located within the excluded area of the first one [23]. The excluded area depends on the mutual orientation of the discorrectangles

$$A_{\text{ex}} = \sin \vartheta (l - d)^2 + 4d(l - d) + \pi d^2, \quad (4)$$

where ϑ is the angle between the two discorrectangles [23, 24] (Fig. 3).

Superposition of the excluded areas for all possible mutual angles between two discorrectangles can be treated as a probability map, i.e., the probability that a randomly oriented discorrectangle will overlap an original discorrectangle. Figure 4 presents the probability map when all orientations are equiprobable (isotropic deposition).

To detect any overlapping of the discorrectangles, we used their midlines (Fig. 5).

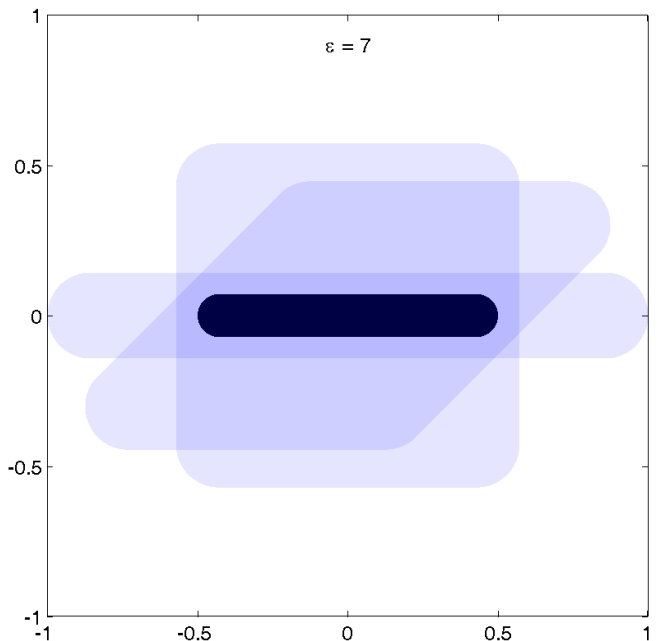


FIG. 3. Examples of the excluded areas of a discorrectangle for different angles between this discorrectangle and a second one; $\vartheta = 0, \pi/4, \pi/2$, $\varepsilon = 7$.

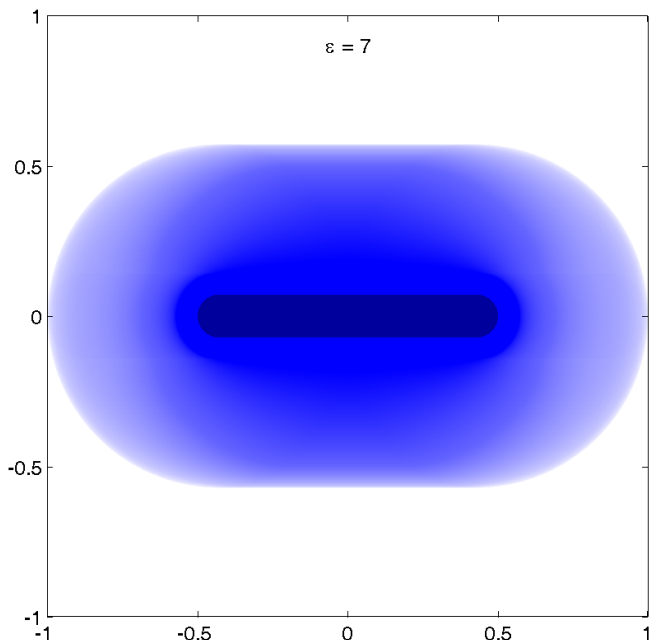


FIG. 4. Example of the probability map when all orientations of the discorrectangles are equiprobable (isotropic deposition of discorrectangles) for $\varepsilon = 7$. The reference discorrectangle is shown. The darkest shade corresponds to the probability 1, i.e., when the center of the second discorrectangle is located within this area, and overlapping of these two discorrectangles is ensured.

1. The discorrectangles overlap, if their midlines intersect each other [Fig. 5(a)].

2. If the two midlines do not intersect each other, but the shortest distance between these midlines is less than the width of the discorectangle, d , the corresponding discorectangles overlap [Fig. 5(b)].
3. If the two midlines do not intersect each other and the shortest distance between these midlines is larger than the width of the discorectangle, d , the corresponding discorectangles do not overlap [Fig. 5(c)].

The limiting cases are obvious. To check whether two zero-width sticks intersect, consideration of just the first item above is enough. The two disks intersect each other when the distance between their centers is less than d .

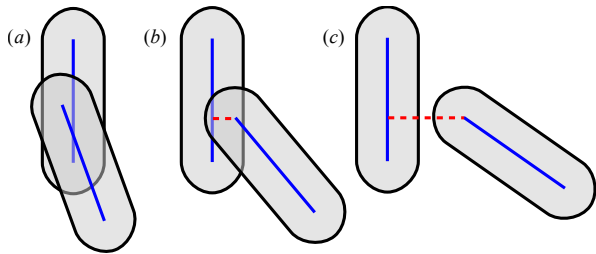


FIG. 5. (a) The discorectangles overlap, since their midlines intersect each other. (b) The discorectangles overlap, since the shortest distance between their midlines is less than the width of the discorectangle, d . (c) The corresponding discorectangles do not overlap, since the shortest distance between their midlines is larger than the width, d , of a discorectangle.

The probability that two identical particles intersect with each other can be found using the excluded area concept [23]

$$P = \frac{A_{\text{ex}}}{L^2}, \quad (5)$$

where, in the case of isotropically-placed discorectangles, the angle-averaged excluded area is

$$\langle A_{\text{ex}} \rangle = \frac{2}{\pi}(l-d)^2 + 4d(l-d) + \pi d^2 \quad (6)$$

(see, e.g., Refs. 23 and 24) or

$$\langle A_{\text{ex}} \rangle = l^2 \left[\frac{2}{\pi}(1 - \varepsilon^{-1})^2 + 4\varepsilon^{-1}(1 - \varepsilon^{-1}) + \pi\varepsilon^{-2} \right] \quad (7)$$

(see, e.g., Ref. 15). In the case of disks ($l = d$, $\varepsilon = 1$),

$$\langle A_{\text{ex}} \rangle = \pi d^2 = \pi l^2, \quad (8)$$

while in the case of zero-width sticks ($d = 0$, $\varepsilon = \infty$),

$$\langle A_{\text{ex}} \rangle = \frac{2l^2}{\pi}. \quad (9)$$

The mean number of intersections per deposited particle is $\langle k \rangle = (N-1)P$ or

$$\langle k \rangle \approx nPL^2, \quad (10)$$

when $N \gg 1$. Hence, the total number of contacts (junctions) between particles is

$$N_j = N \frac{nPL^2}{2} = \frac{n^2 L^2 \langle A_{\text{ex}} \rangle}{2}, \quad (11)$$

while the number density of contacts is

$$n_j = \frac{n^2 \langle A_{\text{ex}} \rangle}{2}. \quad (12)$$

Formula (12) is valid for identical particles of any shape, not only for discorectangles. Moreover, formula (12) is valid for anisotropic systems when the angle-averaged excluded area is calculated using the appropriate angle-distribution function. Thereby, there is a quadratic dependency of the number density of the contacts between the deposited particles on the number density of the deposited particles.

For all values of discorectangle aspect ratio, we used domains of a fixed size $L = 32l$. To efficiently determine the percolation threshold (occurrence of a percolation cluster that spans the system in a given direction), the union-find algorithm [25, 26] was used. Figure 6 exhibits an example of a system under consideration exactly at the percolation threshold. The spanning cluster is highlighted. The aspect ratio of the discorectangles is 7.

We used the normalized number density of the deposited particles, viz., $n/n_c - 1$, in all our figures. Here, n_c is the percolation threshold. Notice that the normalized number density is equal to the normalized total area fraction $\eta/\eta_c - 1$.

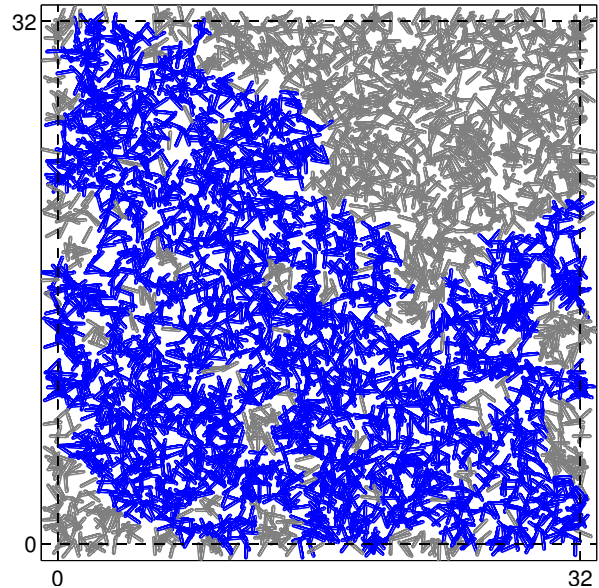


FIG. 6. Example of a system under consideration exactly at the percolation threshold. The spanning cluster is highlighted. The aspect ratio of the discorectangles is 7.

C. Electrical properties

To study the electrical properties of the deposit, we added superconductive busses to the two opposite boundaries of the system under consideration. Only the resistance of junctions between particles was taken into account. This assumption of junction resistance dominance has previously been widely used [12, 16, 22]. In such a way, the system under consideration can be transformed into a network, in which the edges correspond to the contacts (overlaps) between deposited particles, while the vertices of the network correspond to the deposited particles. This network is not planar. In it, each edge represents the resistance R_j (the conductance is σ_j), i.e., a random resistor network (RRN) is being considered. To be precise, there is an irregular network with identical branch resistances. For this particular case of the RRN, some analytical results derived on the basis of the Foster theorem [27, 28] are known [29].

Let y_i be the admittance associated with the i -th branch, while Y_i is the admittance seen from the endpoints of the i -th branch when y_i is disconnected. For an irregular network with identical branch admittances $y_i = y_m$,

$$\left\langle \frac{y_m}{y_m + Y_i} \right\rangle = \frac{2}{\langle \text{deg } V \rangle}, \quad (13)$$

where $\langle \text{deg } V \rangle$ is the average degree of the network nodes [29]. In our case, accounting for Eqs. (10) and (5), $\text{deg } V = \langle k \rangle \approx nA_{\text{ex}}$

$$\left\langle \frac{\sigma_j}{\sigma_j + Y_i} \right\rangle = \frac{2}{nA_{\text{ex}}}. \quad (14)$$

To identify a current-carrying part (the backbone) of the percolation cluster, we used the algorithm as follows (for the sake of clarity some irrelevant details have been omitted).

Let G' be the percolation cluster of the network G . The vertices of G' belonging to one bus are considered as inputs, while the vertices belonging to the other bus are considered as outputs. Initially, all vertices and all edges of the network G' are marked as “unremoved”.

1. Add vertices V_1 and V_2 to the network G' in such a way that V_1 is connected to all the inputs, while V_2 is connected to all the outputs.
2. Find all articulation points.
3. Check each articulation point. If the current articulation point (vertex X) is marked as “unremoved”, then
 - (a) Find all vertices adjacent to X .
 - (b) Mark X and all its incident edges as “removed”.
 - (c) Check each vertex, Y , that is adjacent to X .

i. Check the presence of paths from vertex Y to vertices V_1 and V_2 in the subgraph H , which consists of “unremoved” vertices and edges of the network G' .

ii. If there is a path leading from vertex Y to neither V_1 nor V_2 , then we mark as “removed” all vertices and edges of the connected component of network H containing vertex Y .

4. Mark the vertex X as “unremoved”.

5. Mark as “unremoved” all edges between the vertex X and the vertices marked as “unremoved”.

In fact, we are looking for a geometrical backbone, i.e., a biconnected component of the network. A geometrical backbone can contain perfectly balanced bonds (Wheatstone bridges). Since the potential difference between the ends of a perfectly balanced bond is equal to zero, electrical current through this bond is absent [30]. However, it is intuitively clear that the fraction of perfectly balanced bonds has to be negligible, if there are any at all. By contrast, direct identification of the current-carrying part of the percolation cluster is hardly reliable, since some apparent, but actually non-existent, currents may arise both in dead ends and in perfectly balanced bonds due to rounding-off errors. These currents may be of the same order of magnitude as the real currents in some parts of the network.

A definition for the local transport exponent [12, 16, 31, 32] is

$$t = \frac{d \ln \sigma}{d \ln(\eta - \eta_c)} = \frac{\eta - \eta_c}{\sigma} \frac{d\sigma}{d\eta} = \frac{n - n_c}{\sigma} \frac{d\sigma}{dn}. \quad (15)$$

Using an analytical formula for the electrical conductivity of 2D system of randomly placed conductive sticks that was obtained within a mean-field approach [18]

$$\sigma = \frac{n^2 l^4}{12\pi R_j}, \quad (16)$$

the local transport exponent may be derived as

$$t = 2 \frac{n - n_c}{n}. \quad (17)$$

This local transport exponent tends to 2, when $n \gg n_c$.

The error bars in the figures correspond to the standard deviation of the mean. When not shown explicitly, they are of the order of the marker size.

III. RESULTS

Figure 7 demonstrates the strength of the percolation cluster (filled markers) and its backbone (open markers) against the normalized number density, $n/n_c - 1$, for discorectangles possessing different aspect ratios, i.e., from

disks to sticks. First of all, the results seem to be independent or almost independent of the aspect ratio. However, a small deviation for disks can be noticed. This deviation requires an additional detailed study. Moreover, three different regimes can be observed, viz., (i) a percolation regime ($n \lesssim 1.1n_c$), (ii) a transient regime ($n_c \lesssim n \lesssim 1.7n_c$), and (iii) a bulk regime ($n \gtrsim 1.7n_c$). In the bulk regime, all, or almost all, the particles belong to the percolation cluster. It is noteworthy that universal (aspect ratio invariant) behavior is observed in all three regimes.

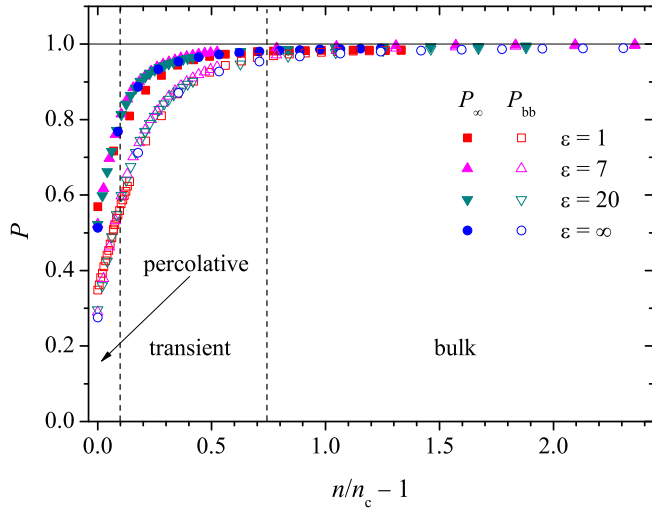


FIG. 7. Strength of the percolation cluster (filled markers) and its backbone (open markers) against the normalized number density, $n/n_c - 1$, for discorightangles having different aspect ratios. The results are averaged over 1000 independent runs.

Figure 8 presents a close look at the behavior of the percolation cluster strength. The strength of the percolation cluster is normalized by the strength of the percolation cluster of the sticks ($\varepsilon = \infty$). For any studied values of the number density, this normalized strength of the percolation cluster approaches unity as the aspect ratio increases.

However, this approach may be nonmonotonic (Fig. 9).

Figure 10 shows the density of particles belonging to the backbone of the percolation cluster, normalized by the density of particles at the percolation threshold, n_c . The filled markers correspond to our results, while the open markers correspond to data extracted from the literature, viz., the data for ellipses (PRB2021) have been adapted from Ref. 12, while the data for sticks (PRB2012) have been adapted from Ref. 16. A noticeable divergence when $n/n_c - 1 \lesssim 0.2$ may arise due to both a finite-size effect and a strong dependency on the accuracy of the percolation threshold estimate. In any case, for $n/n_c - 1 \gtrsim 0.2$, all data collapse to one curve, confirming the proposition about an aspect-ratio-invariant behavior [12]. The inset shows a slight monotonic decrease in

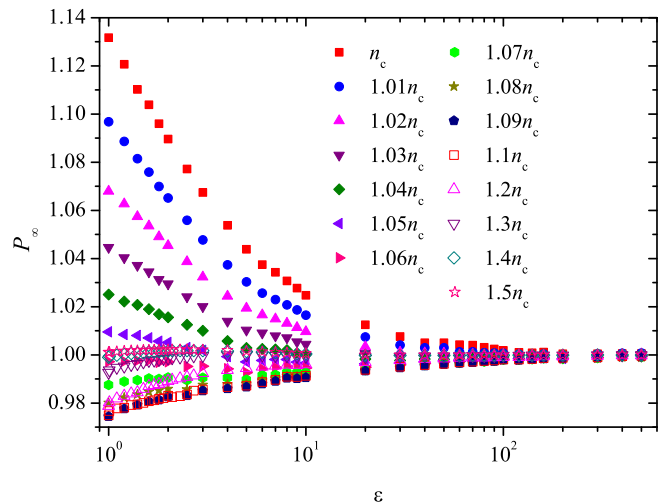


FIG. 8. Strength of the percolation cluster versus the aspect ratio for different values of the number density. The results are averaged over 100 000 independent runs.

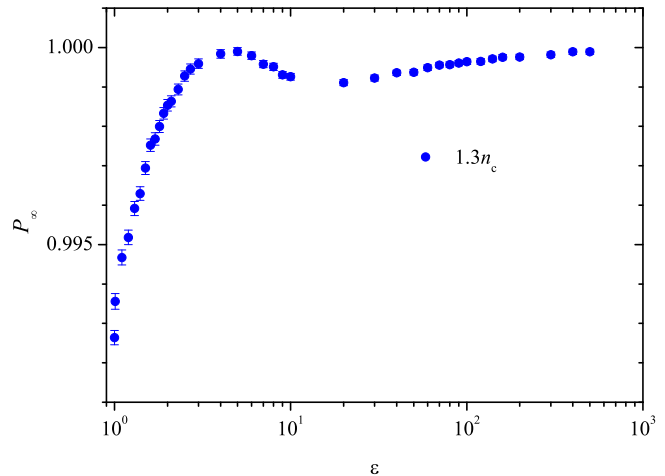


FIG. 9. Strength of the percolation cluster on the aspect ratio for $n = 1.3n_c$. The results are averaged over 100 000 independent runs.

the normalized density of the particles belonging to the backbone of the percolation cluster with an increase in the value of the aspect ratio of the discorightangles for the fixed value of the number density of the particles of $n = 2n_c$. Our results are averaged over 100 independent runs.

Figure 11 demonstrates the density of the junctions or bonds in the backbone normalized by the density of the junctions at the percolation threshold, n_{j_c} . The filled markers correspond to our results, while the open markers correspond to data extracted from the literature, viz., the data for ellipses (PRB2021) have been adapted from Ref. 12, while the data for sticks (PRB2012) have been adapted from Ref. 16. The inset shows that, for the fixed value of the number density $n = 2n_c$, the normalized

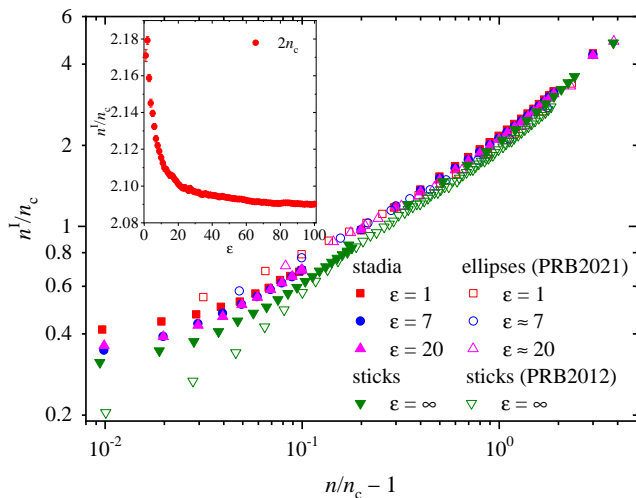


FIG. 10. Density of particles belonging to the backbone of the percolation cluster, normalized by the density of particles at the percolation threshold, n_c . Filled markers correspond to our results, while open markers correspond to data extracted from the literature. PRB2012 refers to Ref. 16, PRB2021 refers to Ref. 12. Inset: dependence of the normalized density of the particles belonging to the backbone of the percolation cluster on the aspect ratio of the discorectangle for the fixed value of the number density of the particles of $n = 2n_c$. Our results are averaged over 100 independent runs.

density of the junctions belonging to the backbone of the percolation cluster decreases as the aspect ratio of the discorectangles is increased from 1 to 5, and remains constant within the error bars with further increase. Our results are averaged over 100 independent runs. Since our results obtained using both geometrical and conductive backbones are consistent within the marker size, only one data set is presented in Fig. 11. All our data collapse to one curve, confirming the proposition of an aspect-ratio-invariant behavior [12]. For $n/n_c - 1 \gtrsim 0.2$, and our results for sticks agree the results presented in Ref. 16. Again, a noticeable divergence when $n/n_c - 1 \lesssim 0.2$ may arise due to both a finite-size effect and a strong dependency on the accuracy of the percolation threshold estimate. However, our results are located significantly above the data for ellipses [12]. The more natural assumption about differences in methods was not confirmed in our discussion with one of the authors of Ref. 12.

Figure 12 compares the behavior of the electrical conductivity for ellipses (filled markers) [12] and discorectangles (open markers). Again, the dependence of the electrical conductivity on the normalized number density seems to be independent of the aspect ratio. Moreover, the dependencies for both the ellipses [12] and the discorectangles collapse to single curve except for a region slightly above the percolation threshold.

Figure 13 presents the behavior of the local transport exponent for ellipses (filled markers) [12] and discorectangles (open markers). Again, the dependence of the

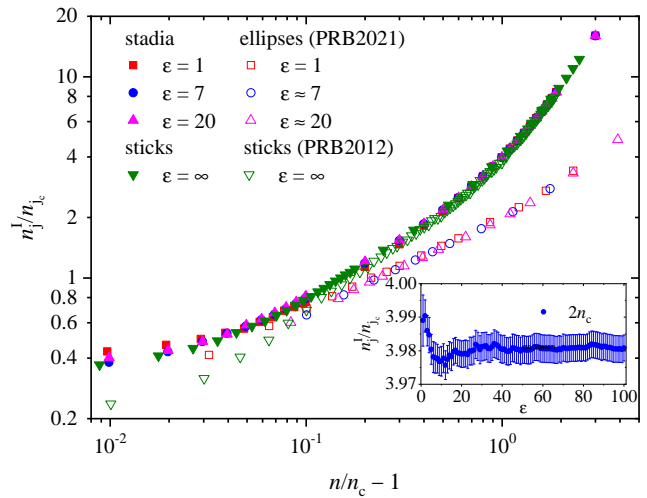


FIG. 11. Density of junctions or bonds in the backbone normalized by the density of junctions at the percolation threshold, n_{j_c} . Filled markers correspond to our results, while open markers correspond to data extracted from the literature. PRB2012 refers to Ref. 16, PRB2021 refers to Ref. 12. Inset: dependence of the normalized density of junctions belonging to the backbone of the percolation cluster on the aspect ratio of the discorectangles for the fixed value of the number density of the particles, $n = 2n_c$. Our results are averaged over 100 independent runs.

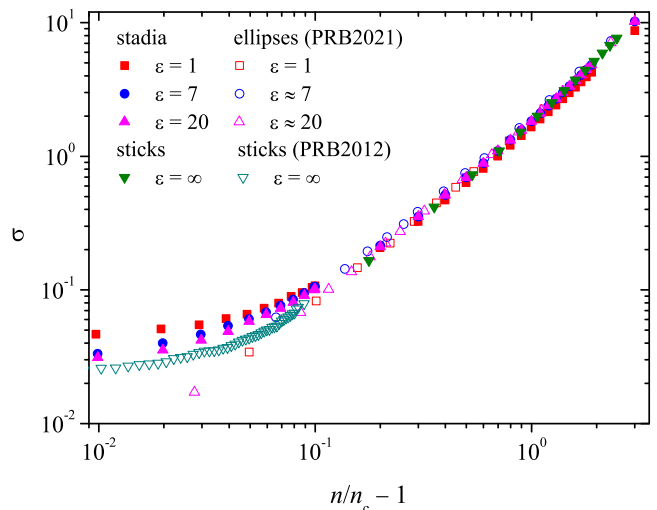


FIG. 12. Electrical conductivity against the normalized number density, $n/n_c - 1$. Filled markers correspond to our results, while open markers correspond to data extracted from the literature. PRB2012 refers to Ref. 16, PRB2021 refers to Ref. 12. Our results are averaged over 100 independent runs.

electrical conductivity on the normalized number density seems to be independent of the aspect ratio. Moreover, the dependencies for both ellipses [12] and discorectangles collapse to single curve. The exponent tends to the analytical prediction (17) when the number density increases.

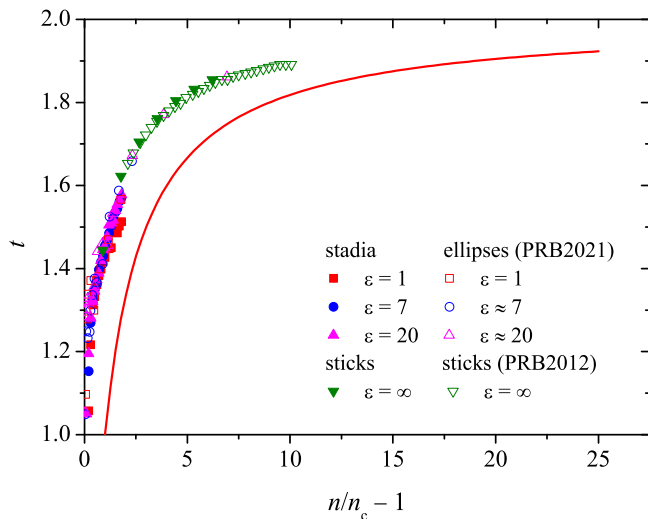


FIG. 13. Local transport exponent against the normalized number density, $n/n_c - 1$. Filled markers correspond to our results, while open markers correspond to data extracted from the literature. PRB2012 refers to Ref. 16, PRB2021 refers to Ref. 12. The solid curve corresponds to Eq. (17). Our results are averaged over 100 independent runs.

IV. CONCLUSION

Recently, the dynamics of 2D disordered systems of ellipses has been simulated [12]. Using a particular definition of the normalized proximity to the percolation threshold, the authors found an eccentricity-invariant dynamic behavior. The authors suggested that this invariance might also arise in systems with other particle geometries having zero-width sticks as the limiting case. To check this suggestion, we performed a study using discorectangles including their limiting cases, viz., disks and zero-width sticks. Our computer simulations demon-

strate that some properties of random isotropic 2D systems of conductive discorectangles are insensitive to the aspect ratio of the particles. Our study presents some arguments that the suggestion may be correct. At least, the behavior of 2D systems of randomly-placed, conductive, permeable discorectangles is fairly close to that reported for ellipses [12]. The only exception was the density of the junctions in the backbone. Although our results differ from the results reported in Ref. [12], in the limit case of sticks, they do coincide with the results reported in Ref. [16]. We suggest this deviation is due to differences in the definitions or algorithms. Unfortunately, our conversation with one of the authors of Ref. [12] did not elucidate any possible source of this deviation. In order to assist readers, we have presented a detailed description of our own algorithm.

Although, slightly above the percolation threshold, the finite-size effect may presumably be significant, as the wide range of the number densities, when the invariant behavior can be observed, implies the invariant behavior is insensitive to the domain size. Moreover, we suppose that the reported “eccentricity-invariant dynamic behavior” may be observed for a wide range of particles, not only for particles having zero-width sticks as their limiting case.

ACKNOWLEDGMENTS

The authors acknowledge funding from the Foundation for the Advancement of Theoretical Physics and Mathematics “BASIS”, grant 20-1-1-8-1. The authors would also like to thank A.G.Gorkun for technical assistance, R.K.Akhunzhanov for discussions, and A. Álvarez-Álvarez for explanations of some technical details of the study [12].

-
- [1] J. Gao, K. Kempa, M. Giersig, E. M. Akinoglu, B. Han, and R. Li, Physics of transparent conductors, *Adv. Phys.* **65**, 553 (2016).
 - [2] H. Sohn, C. Park, J.-M. Oh, S. W. Kang, and M.-J. Kim, Silver nanowire networks: Mechano-electric properties and applications, *Materials* **12**, 2526 (2019).
 - [3] V. H. Nguyen, D. T. Papanastasiou, J. Resende, L. Bardet, T. Sannicolo, C. Jiménez, D. Muñoz-Rojas, N. D. Nguyen, and D. Bellet, Advances in flexible metallic transparent electrodes, *Small* **18**, 2106006 (2022).
 - [4] R. Gupta, K. D. M. Rao, S. Kiruthika, and G. U. Kulkarni, Visibly transparent heaters, *ACS Appl. Mater. Interfaces* **8**, 12559 (2016).
 - [5] Y. Zhang, S.-W. Ng, X. Lu, and Z. Zheng, Solution-processed transparent electrodes for emerging thin-film solar cells, *Chem. Rev.* **120**, 2049 (2020).
 - [6] W. Li, H. Zhang, S. Shi, J. Xu, X. Qin, Q. He, K. Yang, W. Dai, G. Liu, Q. Zhou, H. Yu, S. R. P. Silva, and M. Fahlman, Recent progress in silver nanowire networks for flexible organic electronics, *J. Mater. Chem. C* **8**, 4636 (2020).
 - [7] S. Mertens and C. Moore, Continuum percolation thresholds in two dimensions, *Phys. Rev. E* **86**, 061109 (2012).
 - [8] A. P. Chatterjee, A percolation-based model for the conductivity of nanofiber composites, *J. Chem. Phys.* **139**, 224904 (2013).
 - [9] Y. Y. Tarasevich and A. V. Eserkepov, Percolation of sticks: Effect of stick alignment and length dispersity, *Phys. Rev. E* **98**, 062142 (2018).
 - [10] J. Li and M. Östling, Percolation thresholds of two-dimensional continuum systems of rectangles, *Phys. Rev. E* **88**, 012101 (2013).
 - [11] J. Li and M. Östling, Precise percolation thresholds of two-dimensional random systems comprising overlapping ellipses, *Physica A* **462**, 940 (2016).
 - [12] A. Álvarez-Álvarez, I. Balberg, and J. P. Fernández-

- Álvarez, Invariant percolation properties in some continuum systems, *Phys. Rev. B* **104**, 184205 (2021).
- [13] J. Lin and H. Chen, Measurement of continuum percolation properties of two-dimensional particulate systems comprising congruent and binary superellipses, *Powder Technol.* **347**, 17 (2019).
- [14] Y. Y. Tarasevich and A. V. Eserkepov, Percolation thresholds for discorectangles: Numerical estimation for a range of aspect ratios, *Phys. Rev. E* **101**, 022108 (2020).
- [15] N. I. Lebovka and Y. Y. Tarasevich, Two-dimensional systems of elongated particles: From diluted to dense, in *Order, disorder and criticality: advanced problems of phase transition theory*, Vol. 6, edited by Y. Holovatch (WORLD SCIENTIFIC, Singapore, 2020) Chap. 4, pp. 153–200.
- [16] M. Žeželj and I. Stanković, From percolating to dense random stick networks: Conductivity model investigation, *Phys. Rev. B* **86**, 134202 (2012).
- [17] A. Aryanfar, S. Medlej, A. Tarhini, and A. R. Tehrani B, Elliptic percolation model for predicting the electrical conductivity of graphene–polymer composites, *Soft Matter* **17**, 2081 (2021).
- [18] Y. Y. Tarasevich, I. V. Vodolazskaya, and A. V. Eserkepov, Electrical conductivity of random metallic nanowire networks: an analytical consideration along with computer simulation, *Phys. Chem. Chem. Phys.* **24**, 11812 (2022).
- [19] I. Balberg, N. Binenbaum, and C. H. Anderson, Critical behavior of the two-dimensional sticks system, *Phys. Rev. Lett.* **51**, 1605 (1983).
- [20] C. O’Callaghan, C. Gomes da Rocha, H. G. Manning, J. J. Boland, and M. S. Ferreira, Effective medium theory for the conductivity of disordered metallic nanowire networks, *Phys. Chem. Chem. Phys.* **18**, 27564 (2016).
- [21] C. Forró, L. Demkó, S. Weydert, J. Vörös, and K. Tybrandt, Predictive model for the electrical transport within nanowire networks, *ACS Nano* **12**, 11080 (2018).
- [22] D. Kim and J. Nam, Electrical conductivity analysis for networks of conducting rods using a block matrix approach: A case study under junction resistance dominant assumption, *J. Phys. Chem. C* **124**, 986 (2019).
- [23] I. Balberg, C. H. Anderson, S. Alexander, and N. Wagner, Excluded volume and its relation to the onset of percolation, *Phys. Rev. B* **30**, 3933 (1984).
- [24] A. N. Volkov and L. V. Zhigilei, Thermal conductivity of two-dimensional disordered fibrous materials defined by interfiber thermal contact conductance and intrinsic conductivity of fibers, *J. Appl. Phys.* **127**, 065102 (2020).
- [25] M. E. J. Newman and R. M. Ziff, Efficient Monte Carlo algorithm and high-precision results for percolation, *Phys. Rev. Lett.* **85**, 4104 (2000).
- [26] M. E. J. Newman and R. M. Ziff, Fast Monte Carlo algorithm for site or bond percolation, *Phys. Rev. E* **64**, 016706 (2001).
- [27] R. M. Foster, The average impedance of an electrical network, in *Reissner Anniversary Volume — Contributions to Applied Mechanics*, edited by S. of the Department of Aeronautical Engineering and A. M. of the Polytechnic Institute of Brooklyn (Polytechnic Institute of Brooklyn, Edwards, J. W., Ann Arbor, Mich., 1949) pp. 333–340.
- [28] R. M. Foster, An extension of a network theorem, *IRE Trans. Circuit Theory* **8**, 75 (1961).
- [29] J. Marchant, Effective-medium theory applied to resistor networks: an electrical network theory interpretation, *J. Phys. C: Solid State Phys.* **12**, L517 (1979).
- [30] C. Li and T.-W. Chou, A direct electrifying algorithm for backbone identification, *J. Phys. A: Math. Theor.* **40**, 14679 (2007).
- [31] J. Bernasconi, Real-space renormalization of bond-disordered conductance lattices, *Phys. Rev. B* **18**, 2185 (1978).
- [32] C. Grimaldi and I. Balberg, Tunneling and nonuniversality in continuum percolation systems, *Phys. Rev. Lett.* **96**, 066602 (2006).